Journal of Solid State Electrochemistry (2021) 25:963–972
https://doi.org/10.1007/s10008-020-04864-z

ORIGINAL PAPER

Effect of conductive polypyrrole in poly(acrylonitrile-*co*-butyl acrylate) water–based binder on the performance of electrochemical double-layer capacitors

Yanchunxiao Qi[1] · Minh Hien Thi Nguyen[1] · Eun-Suok Oh[1]

Received: 4 August 2020 / Revised: 24 October 2020 / Accepted: 6 November 2020 / Published online: 19 November 2020

Abstract

Electrochemical double-layer capacitors (EDLCs) have been widely studied due to their high-power densities, despite their low energy densities compared with those of lithium ion batteries. In particular, there have been numerous studies aiming to developing high surface area carbonic material to increase EDLCs' capacitance. However, there have been few studies examining water-based polymeric binder as an inactive component of the EDLCs' electrodes. In this study, we introduce a conductive water-based binder which is synthesized by an in situ two-step polymerization, and use it for EDLC electrodes. Polypyrrole (PPy) is used as an electrically conducting filler for a water-based polyacrylate binder to enhance the electrochemical performance of EDLCs. Consequently, the use of the new poly(pyrrole/acrylonitrile-*co*-butyl acrylate) (PPyANBA) increases the specific capacitance of the EDLC electrode up to 109.7 F g^{-1} from the 101.0 F g^{-1} value of the nonconductive PANBA-containing EDLC electrode at 10,000 cycles. This is mainly attributed to the better dispersion and lower electrical resistance of the PPyANBA binder without losing the thermal, ion transport, and binding characteristics of the PANBA.

Keywords Polypyrrole · Poly(acrylonitrile-*co*-butyl acrylate) · Poly(pyrrole/acrylonitrile-*co*-butyl acrylate) conducting polymer · Water-based binder · Electrochemical double-layer capacitor

Introduction

The recent developments in energy storage systems have attracted the attention of many researchers due to the transition of fossil energy to renewable energy [1–3]. For large-scale applications, such as a hydrogen network, underwater compressed air and solar cells are commonly used, while rechargeable batteries and supercapacitors are used for small, middle-scale, and moveable applications [2, 4, 5]. Among them, supercapacitors, particularly electrochemical double-layer capacitors (EDLCs), are considered promising electrochemical energy storage systems due to their fast charge discharge character, long life expectancy, high power density, and low maintenance [6–9]. Hence, supercapacitors are popularly applied in portable devices, wearable devices, memory backup systems, and braking systems of electric vehicles (EVs) and hybrid electric vehicles (HEVs) [10–14].

✉ Eun-Suok Oh
esoh1@ulsan.ac.kr

[1] School of Chemical Engineering, University of Ulsan, 93 Daehak-ro, Nam-gu, Ulsan 44610, Republic of Korea

In general, the capacitance of an EDLC is highly correlated to the surface area of the active materials. Therefore, carbonaceous materials which have a large surface area, such as activated carbon, have mainly been used for EDLCs [15–17]. For this reason, many researchers focus on increasing the surface area of the active material [18–20], even though other components, such as the conducting agent and the polymer binder, also play crucial roles. The conducting agent helps form continuous electron pathways in electrodes for high-power EDLC [21]. By contrast, the polymeric binder can unite all electrode ingredients and maintain their integrity on the surface of the current collector during the charge and discharge processes, even with a small content of 5–10 wt% compared with the active material [22, 23]. Instead of traditional polyvinylidene fluoride (PVdF) dissolved in toxic *n*-methyl pyrrolidone solvent, water-based binder such as styrene-butadiene rubber (SBR) is mainly used due to its eco-friendly characteristics in the electrode manufacturing process and its superior electrochemical performance [24–27]. Water-treatable polyacrylates are also promising binders because their intrinsic low glass transition temperatures (T_g) lead to a flexible character which can enhance the performance of the

electrodes [28–30]. However, polyacrylates are still electrically nonconductive, which can increase the electrical resistance of EDLCs and ultimately deteriorate their high power characteristics. There are two ways to increase the electrical conductivity of the binder: the direct use of electronically conducting polymers and the addition of conductive filler to nonconducting adhesive polymer.

In previous studies, typical conducting polymers such as polyaniline, polypyrrole (PPy), poly(3,4-ethylenedioxythiophene)/poly(styrene sulfonate), and polythiophene have been applied to EDLCs and lithium ion batteries (LIBs) as the binder of the electrodes [31–33]. Unfortunately, they were not successful because their low adhesion did not maintain the mechanical integrity of the electrodes during the repeated cycles. This is why the conducting polymers are normally combined with adhesive polymer binders, such as carboxymethyl chitosan [34, 35] and polyacrylic acid [29]. Based on the percolation theory, adding conductive nanocarbon fillers into polymer matrix has also been widely investigated to enhance polymer conductivity [36–39]. These conductive composite binders could improve the electrochemical performance of LIBs [30, 40–42]. In this study, instead of using the conductive nanocarbons, we use an electrically conducting polymer, PPy as filler for a water-based polyacrylate binder to enhance the electrochemical performance of EDLCs. PPy is known for its good environment stability and easy synthesis process [43, 44]. Water-dispersed poly(acrylonitrile-*co*-butyl acrylate) (PANBA) is chosen as a polyacrylate binder because it exhibits superior binder performance for LIB anodes [29, 45]. Based on our previous work on allocating the optimal ratio between PPy and PANBA [46], only 1 wt% PPy based on PANBA monomer weight is used in this study. A variety of physical and electrochemical EDLC tests are conducted on the conductive poly(pyrrole/acrylonitrile-*co*-butyl acrylate) (PPyANBA) binder, and the results are compared to those of the nonconductive PANBA binder.

Experimental

Synthesis of poly(pyrrole/acrylonitrile-*co*-butyl acrylate)

Emulsified PPy was first synthesized by emulsion polymerization. A certain amount of sodium dodecyl sulfate (SDS, Tokyo Chemical Industry Co., Japan) emulsifier was added into distilled deionized (DDI) water placed in a jacket reactor. Next, 1 wt% of pyrrole monomer (Alfa Aesar, USA) based on the sum of acrylonitrile (AN, Junsei Chemical Co., Ltd., Japan) and butyl acrylate (BA, Samchun Chemical Co., Ltd., Korea) monomers was added. The polymerization was initiated by adding potassium persulfate (KPS, Sigma-Aldrich, USA) when the temperature reached 70 °C, and it was performed for 2 h at that temperature. Then, the mixture of AN and BA was added into the emulsified PPy solution to polymerize PANBA in the PPy emulsion. More details on this step are available in our previous work [29]. The final product, called PPyANBA, was cooled down to room temperature.

Manufacture of EDLCs' electrodes and coin-full cells

Solid in electrode slurry was composed of 91.5 wt% of activated carbon (YP-50F, Kuraray Chemical Co., Ltd., Japan), 2.5 wt% of super-p (Alfa Aesar, USA) conducting agent, 1.5 wt% of carboxymethyl cellulose (CMC, Daicel Fine Chem Ltd., Japan) thickener, and 4.5 wt% of emulsified binder. The slurry was mixed in a Thinky mixer (MD BROS Co., Ltd., Japan), coated on etching aluminium foil, and dried in a convection oven (OF-12GW JE10 TECH, Korea) at 60 °C for 30 min. The electrode was dried again in a vacuum oven (OV-11 JE10 TECH, Korea) at 70 °C for 24 h to remove the remaining water just before use. The thickness of the electrodes was 105 ± 5 μm. The mass loading of the activated carbon on electrode was 6.45 ± 0.5 mg. Using the electrodes, a symmetry type of CR2032 coin cell (Wlcos Corporation, Korea) was assembled in an argon-filled glove box with a polypropylene film separator (Wlcos Corporation, Korea) placed between the symmetric electrodes. Here, 1 M tetraethylammonium tetrafluoroborate in acetonitrile was used as the electrolyte.

Physical and electrochemical characterization of binders and electrodes

The physical stability of the binder solution was recorded using a Turbiscan station (Turbiscan LAB, Formulaction Co., France). The functional groups of the synthesized polymer were confirmed by Fourier transform infrared spectroscopy (FTIR, Nicolet iS5 Thermo Fisher Scientific, USA). The electrical resistances of the binders were measured using electrochemical impedance spectroscopy (EIS, VSP, BioLogic Science Instruments, France) at a frequency range from 10^5 Hz to 10 Hz at 0 V. Thermogravimetric analysis (TGA) and differential scanning calorimetry (DSC) were performed by a Q50 TA Instrument (Discovery TGA35, DSC-PC100, Canada) with a heating rate of 10 °C min^{-1} under nitrogen atmosphere. The zeta potential of the polymer solution was also measured using a Zetasizer Nano ZS (ZEN3600, Malvern Instruments Ltd., UK). The wettability of the binder films, represented by the contact angle of an electrolyte droplet on binder film, was measured using an optical tensiometer (Theta Lite, Biolin Scientific, Japan). The adhesion strength of the electrode was measured by the 180° peel strength of 2-cm-wide electrode strips in a texture analyzer (TA-Plus, Lloyd Instruments Ltd., USA) at a propagation speed of 60 mm min^{-1}. The information on the surface area and pores of the electrodes was obtained from Brunauer-Emmett-Teller (BET)

analysis with N_2 adsorption/desorption at − 196 °C on a surface area and porosity analyzer (Micromeritics ASAP 2020, USA). The degas treatment was maintained at 300 °C for 20 h before analysis. The Barrett-Joyner-Halenda (BJH) and t-plot methods were selected to analyze the pore information of the electrode components. The surface and interface resistivities of the electrode were obtained using a multipoint probe system (RM2610, HIOKI Corp., Japan) at room temperature.

EIS with a frequency range from 10^6 to 10^{-2} Hz at $E = 0$ V was again used to obtain the kinetic parameters related to the charge/discharge processes of long-cycled electrodes. Cyclic voltammetry (CV) testing was also conducted in a battery cycler (WBCS3000, Wonatech, Korea) at several scan rates of 5, 20, 50, and 100 mV s^{-1} between 3.0 V and 0.0 V. The galvanostatic charge/discharge and rate capability tests were also characterized in a battery cycler (PEBC 0550.1, PNE solution Co., Korea) with a constant current and a constant voltage mood at room temperature. For galvanostatic charge/discharge performance, the cells were fully charged/discharged between 2.7 V and 0.1 V at the current of 1.54 mA for the first five cycles. Subsequently, the cells were charged/discharged between 2.7 V and 1.35 V at 4.0 mA for the next 10,000 cycles. Various charge/discharge current densities within 0.5–50 mA cm^{-2} were applied in the rate capability test.

Results and discussion

From the viewpoint of commercial application, the polymeric binder should be physically stable during storage for at least a couple of months. Therefore, above all, it is necessary to check the physical stability of polymer emulsion before it is applied to EDLC electrodes. Very similar to the results of our previous work [30], the Turbiscan station was used for the long-term stability of the binder solution, and the result is represented by the turbiscan stability index (TSI) shown in Fig. S1 of the supplementary information. The low TSI value of the PPyANBA solution demonstrates that it is more stable than the PANBA solution and is suitable to be stored for a couple of months. Additionally, the zeta potentials of the solutions confirm the better stability of the PPyANBA emulsion than the PANBA emulsion. The zeta potential value of the PPyANBA is − 52.4 mV, whereas that of the PANBA is − 45.7 mV. Here, the negative values are originated from the anionic surfactant SDS surrounding the polymer particles. The larger the absolute value of the zeta potential, the stronger the electrostatic force among particles. Thus, the PPyANBA particles are more stabilized in the emulsion due to their strong electrostatic repulsion.

The particle sizes of the binder solutions were first investigated through a zeta potential analysis, and the results are shown in Fig. 1. Both PANBA and PPyANBA particles show

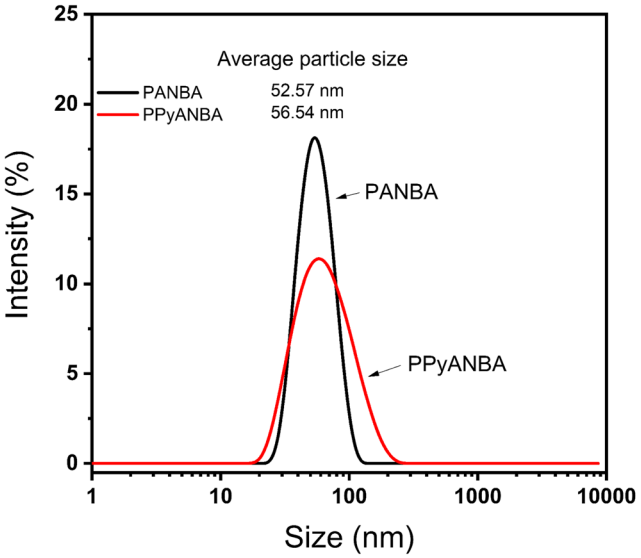

Fig. 1 Particle size distribution of the PANBA and PPyANBA binders

single intensity peaks, indicating that the emulsion polymerization technique is appropriate for synthesizing uniform nanosized polymer particles. Compared with PANBA, the PPyANBA polymer has a wider particle size distribution and a slightly larger average particle size. As shown in Fig. S2, the PPy sample shows a very narrow size distribution and an average size of 37 nm. Therefore, the wide and large characteristic of the PPyANBA implies that the polymerization of PANBA is initiated in PPy micelles and successfully forms the PPyANBA.

Furthermore, the successful synthesis of PPyANBA is also confirmed from the FTIR spectra of the PPy, PANBA, and PPyANBA binder films, as shown in Fig. 2, with those of polyacrylonitrile (PAN) and polybutylacrylate (PBA). The characteristic peaks of PPy are visible at 1168 cm^{-1} and 1644 cm^{-1} for C=N, at 1464 cm^{-1} and 1537 cm^{-1} for C=C, and at 1300 cm^{-1} for C–N [47, 48]. As shown in the FT-IR spectra of PAN and PBA, the characteristic peaks of PANBA at 1780 cm^{-1} and 2240 cm^{-1} are assigned to the stretching vibrations of carbonyl groups in butyl acrylates and of nitrile groups in acrylonitrile, respectively [49, 50]. All the above peaks are present in the PPyANBA spectrum, which implies that the in situ emulsion polymerization of PPyANBA is successfully achieved.

The thermal characteristic of the synthesized binders is investigated by DSC and TGA analyses, and the results are displayed in Fig. 3. Due to the relatively high T_g of PPy ranging between 65 and 95 °C [51], the T_g of PPyANBA slightly increases to 6.6 °C from 4.5 °C of PANBA. Such a low increase does not substantially change the rubbery state of the emulsified binders because the electrode works normally at room temperature, which is much higher than the T_g. In addition, as shown in Fig. 3b, the thermal stability of the binders is almost unchanged by the in situ polymerization of PANBA

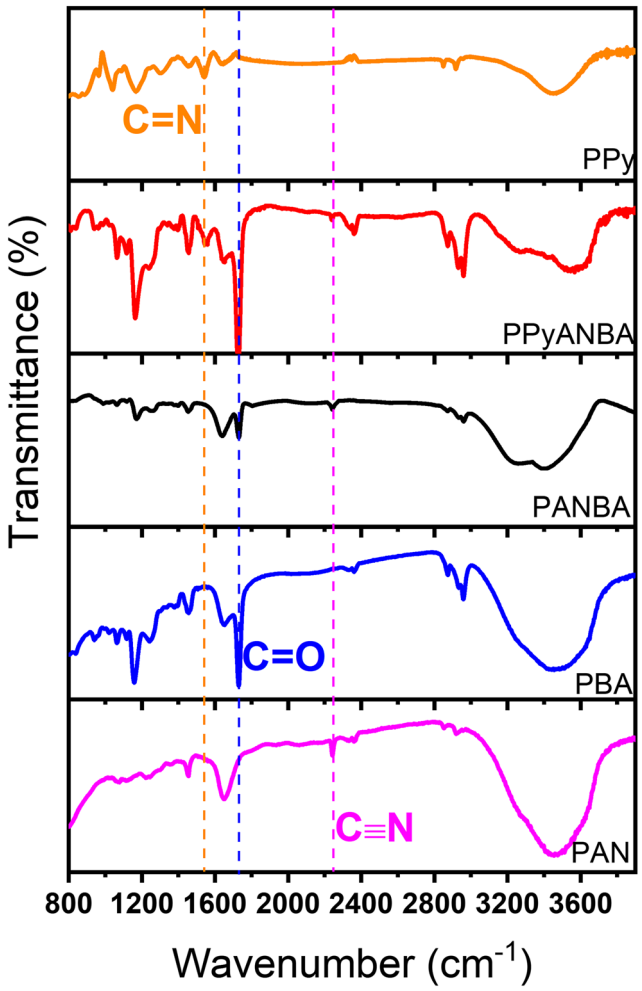

Fig. 2 FTIR spectra of PPy, PAN, PBA, PANBA, and PPyANBA binder films

within PPy emulsion. Both PANBA and PPyANBA are thermally stable up to 350 °C. By contrast, the PANBA mixed physically with the same amount of PPy as PPyANBA shows considerably larger weight loss between 200 and 300 °C compared with those of both PABNA and PPyANBA. The temperature corresponds to the decomposition of PPy [46]. In summary, this in situ emulsion polymerization is an efficient way to introduce a conducting polymer into a rubbery nonconducting polymer without losing its thermal characteristics.

The advantage of introducing conducting PPy into nonconducting PANBA was first observed from EIS, tested at a frequency from 10^5 to 10 Hz, of separated binder films without active materials and electrolyte. The binder film was placed in CR2032 cells with the stainless metal spacer. The EIS analysis indicates that the cell can be simulated as a resistor and a capacitor in series, respectively, as illustrated in Fig. 4. The electrical resistances of the binder samples are determined by linearly extrapolating the impedance to the *x*-axis by increasing the frequency up to infinity [52]. From the linear extrapolation, the electrical resistances of PANBA and PPyANBA are 2.35 kΩ and 1.04 kΩ, respectively. This reveals that conductive PPy works well in PPyANBA, even though a very small amount exists in the PPyANBA sample. Therefore, when compared with pure PANBA, the PPyANBA is favorable for electron transport when applied to the binder for EDLC electrodes. As expected, on the other hand, almost no change occurred in the electrolyte wetting of the binder films, which is closely related to ion transport. The contact angles between binder films and electrolyte droplet recorded at 40 s are very close to each other (Fig. S3 in the supplementary information).

In general, the specific surface area (SSA) and the porosity characteristic of the electrode affect the electrochemical performance of EDLCs. In particular, a large SSA can provide more space for charge storage and thus leads to a higher capacitance [53]. The EDLC electrode powders containing PANBA or PPyANBA binder have been degassed at 300 °C for 24 h before BET analysis. The results of nitrogen sorption isotherms performed at 77 K are shown in Fig. S4(a). Both of

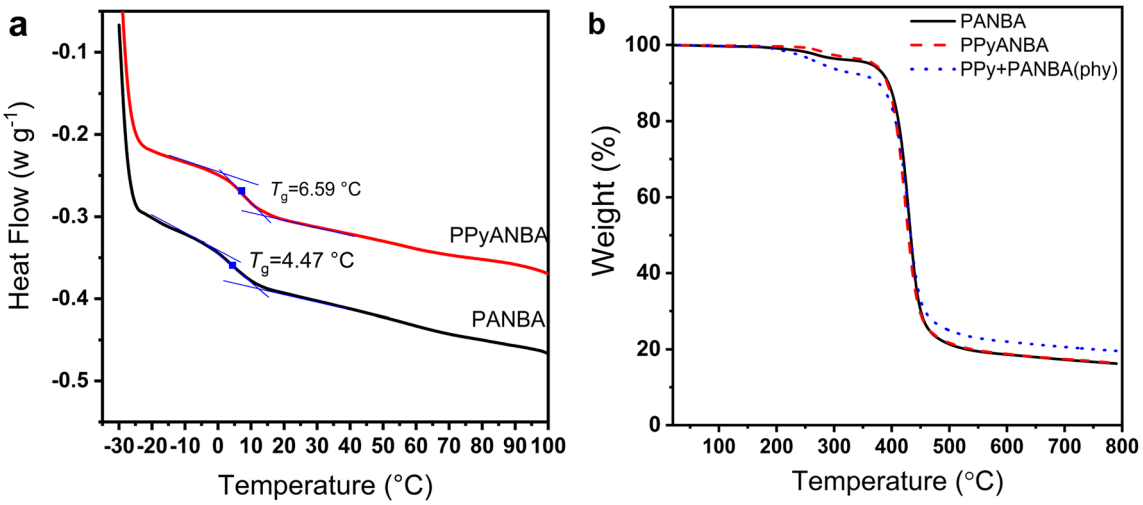

Fig. 3 **a** DSC and **b** TGA of the polymer films. Here, PPy+PANBA(phy) indicates the PANBA mixed physically with 1 wt% PPy

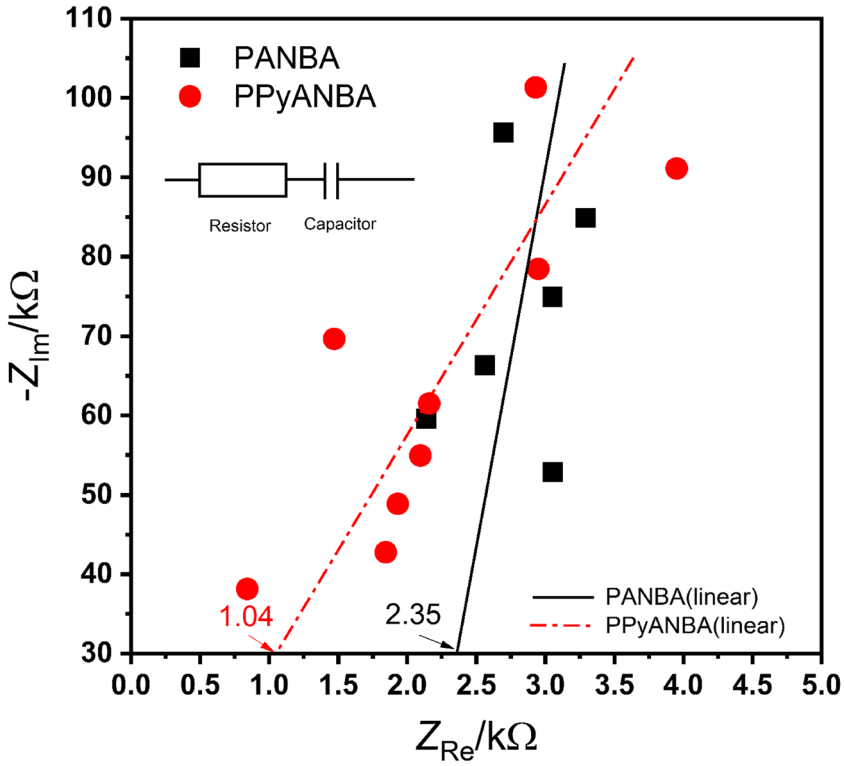

Fig. 4 Nyquist plot of the polymer films to estimate their electrical resistance

the electrodes exhibit mainly type I isotherm curves combined with type IV behavior. The dramatic increase in the isotherm curves at a relatively low pressure (P/P_0 < 0.1) is attributed to the presence of a large number of micropores. The H4 hysteresis loops in the range of P/P_0 = 0.4–0.9 indicate the presence of a small number of mesopores [54]. These are confirmed from Fig. S4(b) and Table 1. Figure S4(b) exhibits their pore size distribution measured using the BJH method. The electrodes are mainly composed of both micropores (d < 2 nm) and mesopores (d = 2–50 nm) without any sensible difference. The majority of mesopores are located between 3.0 and 4.5 nm regardless of the binders. More clear data on the SSA of the pores are listed in Table 1. The PPyANBA-containing electrode powder has higher SSA than the PANBA-containing electrode, even though the PPyANBA binder has a slightly larger size than the PANBA binder, as shown in Fig. 1. In general, bigger binder particles may block larger amounts of pores in the electrode powders. Therefore, the higher SSA of the PPyANBA-containing electrode powder may be attributed to the improved dispersion of the PPyANBA binder particles proven by the zeta potential and TSI values presented in Fig. S1, leading to the homogeneous dispersion and less blocking of binder particles in the electrode, and thus, higher SSA.

The effect of using a conducting PPyANBA binder on the electrical conductivity of the electrode was investigated through 46 multipoint probes connected to an electrode resistance measurement system (RM2610, HIOKI). This system can remove the geometric correction factors required for typical four-point probe systems, such as a significantly larger sample than the probe spacing and a sample thinner than 40% of the probe spacing. Additionally, this system can measure the interface resistance between the electrode composite and the current collector as well as the volume and surface resistivities of the electrode composite. These values of the EDLC electrodes are summarized in Table 2. It is clear that the addition of the conductive PPy to the PANBA binder also improves the electronic conductions of the electrodes and of

Table 1 BET surface areas and pore volumes of EDLC electrode powders.

	S_{BET} ($m^2\ g^{-1}$)	S_{micro} ($m^2\ g^{-1}$)	S_{meso} ($m^2\ g^{-1}$)	Pore V_{total} ($cm^3\ g^{-1}$)
PANBA	1517	1222	295	0.70
PPyANBA	1585	1280	305	0.72

Table 2 Volume and surface resistivities of the electrode composite and the resistance of the interface between the composite and the current collector

Binder-containing electrodes	PANBA	PPyANBA
Composite surface resistivity (mΩ cm^2)	28.2	18.4
Composite volume resistivity (Ω cm)	3.32	2.17
Interface resistance (Ω cm^2)	1.26	0.81

the binder itself. Furthermore, the use of the conductive PPyANBA binder diminishes the interface resistance compared with the nonconductive PANBA binder.

The CV was applied to the EDLC electrodes to observe changes in the basic electrochemical characteristics according to the binder before investigating their cyclic performance. The cyclic voltammetry (CV) test was performed in the range of 0 V to 3 V at the scan rates of 5 mV s^{-1}, 20 mV s^{-1}, 50 mV s^{-1}, and 100 mV s^{-1}, respectively, and the results are shown in Fig. S5. As expected, all voltammograms show typical rectangular shapes with no faradaic peak, indicating capacitive behaviors of the EDLCs regardless of the scan rates. This also indicates that the charges exchange freely in the electrolyte during the positive/negative sweep signals [55].

The cyclic performance of the EDLCs containing different binders was performed with a 4.0 mA current for up to 10,000 cycles, and the results are shown in Fig. 5. The initial and the 10,000th-cycled specific capacitances of the EDLC electrode containing the conductive PPyANBA binder are 133.7 F g^{-1} and 109.7 F g^{-1}, respectively, which are both considerably larger than those for the electrode containing the nonconductive PANBA binder (122.2 F g^{-1} for the 1st and 101.0 F g^{-1} for the 10,000th cycles). This must contribute to the increase in SSA, particularly in the mesopores, and the decrease in the electrical resistance due to the use of the conductive binder, as summarized in Tables 1 and 2. Additionally, the advantage of using the conductive PPy component in the binder was also confirmed through EIS measurement, as shown in Fig. 5b. Though a simple comparison on the cyclic performance of EDLCs may not be appropriate due to its dependence on various factors, the results are compared with previous results reported recently in literature. As shown in Table 3, the PPyANBA binder-containing EDLC has higher cyclic capacitance with considerably good cyclic capacitance retention.

Although there are multiple interpretations of the Nyquist plots of EDLCs, with some even being controversial, EIS analysis can provide information on the resistances of the electrodes. Figure 5b illustrates the effect of the binder on the impedance of EDLC electrodes. R_1 and R_2 are the first and second x-intercepts of the Nyquist plot, respectively, and the resistance R_2 is the sum of the resistance R_1 at a high frequency and the resistance of the semicircle at the middle frequency range. Despite the existence of multiple interpretations, it is generally accepted that the resistance R_2, the so-called internal resistance, is the sum of the bulk electrolyte resistance, the contact resistances between the active materials in the electrode as well as between the electrode and current collector, and the electrolyte resistance in the pores of the

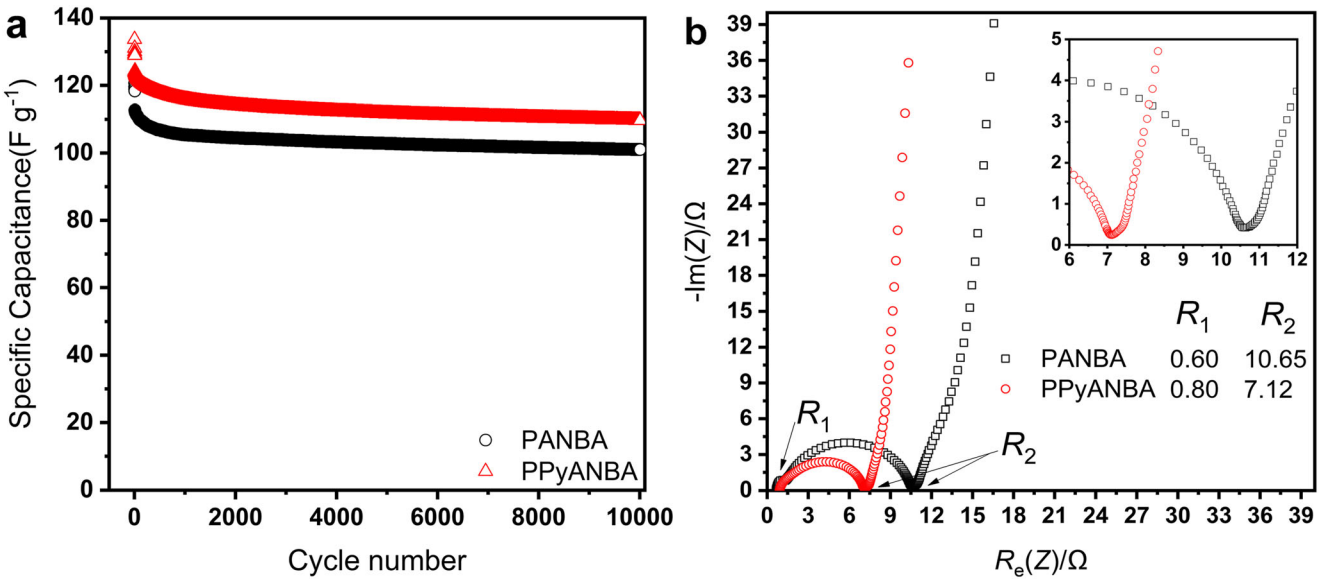

Fig. 5 **a** Cycling performances of EDLC electrodes and **b** Nyquist plots of the EDLCs containing different binders. Here, the 5-cycled EDLCs were used for EIS experiments for the Nyquist plot

Table 3 Comparation with previous results in literature. Here, all of the EDLCs used the same active material, YP-50F

Binder	Cycle number	Final cyclic capacitance (F g^{-1})	Capacitance retention (%)	Energy density (Wh kg^{-1})	Reference
PTFE	2000	90.0	96.0	19.5	[56]
PVDF	10,000	≈ 73.0	91.9	15.8	[57]
PTFE	5000	≈ 80.0	94.7	~ 18.8	[58]
CMC + SBR	5000	< 60.0	78.0	~ 10.0	[59]
PANBA	10,000	101.0	89.6	25.6	This work
PPyANBA	10,000	109.7	88.5	27.8	This work

electrode. The equivalent series resistance (ESR) and the charge transfer resistance are often used to cover the above resistances [60]. As shown in Fig. 5b, the internal resistance of the EDLC cell containing the conductive PPy component in the binder decreases by nearly 33% from 10.6 Ω for the sample without PPy to 7.15 Ω.

As the final investigation of the binder, rate capability tests of the EDLC cells were conducted at a series of current densities (0.5 mA cm^{-2}, 1.0 mA cm^{-2}, 5.0 mA cm^{-2}, 10 mA cm^{-2}, and 50 mA cm^{-2}), and the results are shown in Fig. 6. Twenty cycles per each current density of charge and discharge were carried out between 0.1 and 2.7 V. As expected from the cyclic performance shown in Fig. 5a, the PPyANBA binder increased the specific capacitance of the EDLC at moderate current densities below 10 mA cm^{-2}. However, the highest current density of 50 mA cm^{-2} made the capacitance lower when the conductive PPy component was added in the binder, even though the difference is not so big. This was unexpected because the conductive binder was thought to be more favorable at such a high current density than at low current densities due to its easier electron transport in EDLC. One possible explanation on this phenomenon may be related to the electrode adhesion shown in Fig. 6b. Due to the rapid ion and electron transport, the electrodes are damaged when they are exposed to high current charge/discharge; this damage is more severe in low adhesive electrodes. The introduction of PPy to the PANBA binder lowered the adhesion slightly, thus leading to smaller capacitance of the EDLC only at the high current density when compared with PANBA itself. However, the worse high-rate performance of PPyANBA may not be simply explained by the difference in the electrode adhesion. This could be also affected by other factors such as electrolyte wetting, ionic transport, distribution of binder particles, and so on. Nevertheless, it should be noted that the excess decrease in binder adhesion as a basic characteristic of the binder cannot be compromised with any other binder properties. The use of 1 wt% of PPy in the PANBA binder was able to improve the performance of EDLCs without considerable loss of the binding properties of the PANBA.

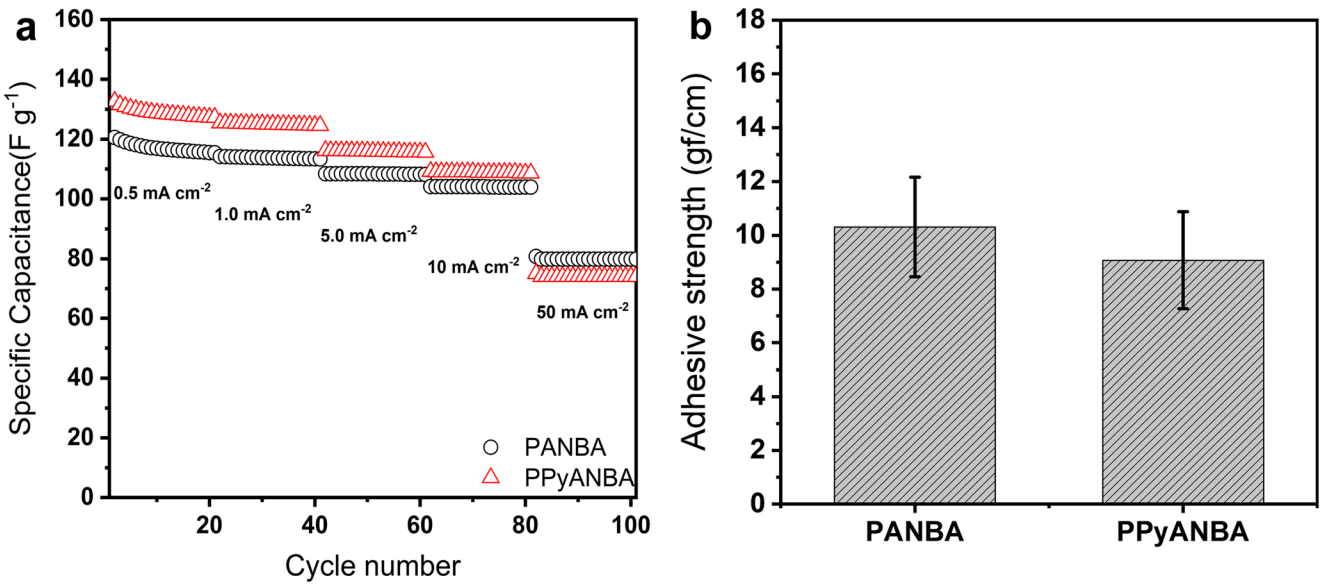

Fig. 6 **a** Rate capability performances of the EDLCs at various current densities. **b** Adhesion strength measured by 180° peel of the electrodes with error bars

Conclusion

The conductive polymer composite poly(pyrrole/acrylonitrile-*co*-butyl acrylate) (PPyANBA) has been successfully synthesized by an in situ two-step emulsion polymerization with PPy as a conductive filler and PANBA as a main polymer matrix, as well as applied to EDLCs as the water-based binder, where it has shown promising electrochemical performance. The first step is to polymerize pyrrole in water medium, followed by the emulsion polymerization of poly(acrylonitrile-*co*-butyl acrylate) using the water-dispersed polypyrrole. The emulsion polymerization is a good way to polymerize the conductive polymer composite, because the continuous stirring force is able to form uniform polymer particles and a long-term stable polymer solution without sacrificing thermal stability. These polymer particles have a good distribution as well as less electrode pore blocking, which is beneficial for EDLCs cycling performance. The conductive polymer composite binder PPyANBA decreases not only the electrodes resistance but also the interface resistance between the electrode and the current collector. Furthermore, charges can be also moved easier in electrode pores with the PPyANBA binder when alternative current is applied. Overall, the EDLCs containing the conductive PPyANBA binder are superior to those containing the nonconductive PANBA binder in long-term cycles at moderate current densities up to 10 mA cm^{-2}.

Supplementary Information The online version contains supplementary material available at https://doi.org/10.1007/s10008-020-04864-z.

Funding The work was supported by the National Research Foundation of Korea grant funded by the Ministry of Science and ICT (MSIT) (NRF-2019R1A2C1004593) and by the Industrial Strategic Technology Development Program funded by the Ministry of Trade, Industry and Energy (MOTIE, Korea) (20009866).

References

1. Bresser D, Hosoi K, Howell D, Li H, Zeisel H, Amine K, Passerini S (2018) Perspectives of automotive battery R&D in China, Germany, Japan, and the USA. J Power Sources 382:176–178. https://doi.org/10.1016/j.jpowsour.2018.02.039
2. Yang Z, Zhang J, Kintner-Meyer MCW, Lu X, Choi D, Lemmon JP, Liu J (2011) Electrochemical energy storage for green grid. Chem Rev 111(5):3577–3613. https://doi.org/10.1021/cr100290v
3. Kim H, Hong J, Park K-Y, Kim H, Kim SW, Kang K (2014) Aqueous rechargeable Li and Na ion batteries. Chem Rev 114(23):11788–11827. https://doi.org/10.1021/cr500232y
4. Liu J, Wang J, Xu C, Jiang H, Li C, Zhang L, Lin J, Shen ZX (2018) Advanced energy storage devices: basic principles, analytical methods, and rational materials design. Adv Sci 5(1):1700322. https://doi.org/10.1002/advs.201700322
5. Soloveichik GL (2011) Battery technologies for large-scale stationary energy storage. Annu Rev Chem Biomol Eng 2(1):503–527. https://doi.org/10.1146/annurev-chembioeng-061010-114116
6. Fong KD, Wang T, Smoukov SK (2017) Multidimensional performance optimization of conducting polymer-based supercapacitor electrodes. Sustain Energy Fuels 1(9):1857–1874. https://doi.org/10.1039/C7SE00339K
7. Kötz R, Carlen M (2000) Principles and applications of electrochemical capacitors. Electrochim Acta 45(15-16):2483–2498. https://doi.org/10.1016/S0013-4686(00)00354-6
8. Winter M, Brodd RJ (2004) What are batteries, fuel cells, and supercapacitors? Chem Rev 104(10):4245–4270. https://doi.org/10.1021/cr020730k
9. Afif A, Rahman SM, Tasfiah Azad A et al (2019) Advanced materials and technologies for hybrid supercapacitors for energy storage—a review. J Energy Storage 25:100852. https://doi.org/10.1016/j.est.2019.100852
10. Wen Z, Yeh M-H, Guo H, Wang J, Zi Y, Xu W, Deng J, Zhu L, Wang X, Hu C, Zhu L, Sun X, Wang ZL (2016) Self-powered textile for wearable electronics by hybridizing fiber-shaped nanogenerators, solar cells, and supercapacitors. Sci Adv 2(10): e1600097. https://doi.org/10.1126/sciadv.1600097
11. Hu Y, Cheng H, Zhao F, Chen N, Jiang L, Feng Z, Qu L (2014) All-in-one graphene fiber supercapacitor. Nanoscale 6(12):6448–6451. https://doi.org/10.1039/C4NR01220H
12. Ke Q, Wang J (2016) Graphene-based materials for supercapacitor electrodes——a review. J Mater 2(1):37–54. https://doi.org/10.1016/j.jmat.2016.01.001
13. Kaempgen M, Chan CK, Ma J, Cui Y, Gruner G (2009) Printable thin film supercapacitors using single-walled carbon nanotubes. Nano Lett 9(5):1872–1876. https://doi.org/10.1021/nl8038579
14. Taberna P-L, Chevallier G, Simon P, Plée D, Aubert T (2006) Activated carbon–carbon nanotube composite porous film for supercapacitor applications. Mater Res Bull 41(3):478–484. https://doi.org/10.1016/j.materresbull.2005.09.029
15. Li X, Wei B (2013) Supercapacitors based on nanostructured carbon. Nano Energy 2(2):159–173. https://doi.org/10.1016/j.nanoen.2012.09.008
16. Pandolfo AG, Hollenkamp AF (2006) Carbon properties and their role in supercapacitors. J Power Sources 157(1):11–27. https://doi.org/10.1016/j.jpowsour.2006.02.065
17. Burke A (2000) Ultracapacitors: why, how, and where is the technology. J Power Sources 91(1):37–50. https://doi.org/10.1016/S0378-7753(00)00485-7
18. Leitner K, Lerf A, Winter M, Besenhard JO, Villar-Rodil S, Suárez-García F, Martínez-Alonso A, Tascón JMD (2006) Nomex-derived activated carbon fibers as electrode materials in carbon based supercapacitors. J Power Sources 153(2):419–423. https://doi.org/10.1016/j.jpowsour.2005.05.078
19. Zhang LL, Zhao XS (2009) Carbon-based materials as supercapacitor electrodes. Chem Soc Rev 38(9):2520–2531. https://doi.org/10.1039/B813846J
20. Lee J, Kim J, Hyeon T (2006) Recent progress in the synthesis of porous carbon mMaterials. Adv Mater 18(16):2073–2094. https://doi.org/10.1002/adma.200501576
21. Wang R, Qian Y, Li W et al (2018) Performance-enhanced activated carbon electrodes for supercapacitors combining both graphene-modified current collectors and graphene conductive additive. Materials (Basel) 11. https://doi.org/10.3390/ma11050799
22. Zhu Z (2016) Effects of various binders on supercapacitor performances. Int J Electrochem Sci 11:8270–8279. https://doi.org/10.20964/2016.10.04
23. Zheng H, Yang R, Liu G, Song X, Battaglia VS (2012) Cooperation between active material, polymeric binder and conductive carbon additive in lithium ion battery cathode. J Phys Chem C 116(7): 4875–4882. https://doi.org/10.1021/jp208428w
24. Bresser D, Buchholz D, Moretti A, Varzi A, Passerini S (2018) Alternative binders for sustainable electrochemical energy storage—the transition to aqueous electrode processing and bio-derived polymers. Energy Environ Sci 11(11):3096–3127. https://doi.org/10.1039/C8EE00640G

25. Yabuuchi N, Kinoshita Y, Misaki K, Matsuyama T, Komaba S (2015) Electrochemical properties of LiCoO2 electrodes with latex binders on high-voltage exposure. J Electrochem Soc 162(4): A538–A544. https://doi.org/10.1149/2.0151504jes
26. Buqa H, Holzapfel M, Krumeich F, Veit C, Novák P (2006) Study of styrene butadiene rubber and sodium methyl cellulose as binder for negative electrodes in lithium-ion batteries. J Power Sources 161(1):617–622. https://doi.org/10.1016/j.jpowsour.2006.03.073
27. Zhang R, Yang X, Zhang D, Qiu H, Fu Q, Na H, Guo Z, du F, Chen G, Wei Y (2015) Water soluble styrene butadiene rubber and sodium carboxyl methyl cellulose binder for ZnFe2O4 anode electrodes in lithium ion batteries. J Power Sources 285:227–234. https://doi.org/10.1016/j.jpowsour.2015.03.100
28. Yoshio M, Brodd RJ, Kozawa A (2009) Lithium-ion batteries: Science and Technologies. Springer-Verlag, New York
29. Nguyen MHT, Oh E-S (2013) Application of a new acrylonitrile/butylacrylate water-based binder for negative electrodes of lithium-ion batteries. Electrochem Commun 35:45–48. https://doi.org/10.1016/j.elecom.2013.07.042
30. Nguyen MHT, Sugartseren N, Kim B, Jeon S, Cho YH, Kim T, Oh ES (2019) Enhancing the electrochemical performance of lithium ion battery anodes by poly(acrylonitrile–butyl acrylate)/graphene nanoplatelet composite binder. J Appl Electrochem 49(4):389–398. https://doi.org/10.1007/s10800-019-01289-z
31. Ajit S, Palaniappan S, Gopukumar S (2013) Polyaniline binder for functionalized acetylene black: a hybrid material for supercapacitor. Synth Met 180:43–48. https://doi.org/10.1016/j.synthmet.2013.07.022
32. Das PR, Komsiyska L, Osters O, Wittstock G (2015) PEDOT: PSS as a functional binder for cathodes in lithium ion batteries. J Electrochem Soc 162(4):A674–A678. https://doi.org/10.1149/2.0581504jes
33. Higgins TM, Park S-H, King PJ, Zhang C(J), McEvoy N, Berner NC, Daly D, Shmeliov A, Khan U, Duesberg G, Nicolosi V, Coleman JN (2016) A commercial conducting polymer as both binder and conductive additive for silicon nanoparticle-based lithium-ion battery negative electrodes. ACS Nano 10(3):3702–3713. https://doi.org/10.1021/acsnano.6b00218
34. Zhong H, He A, Lu J, Sun M, He J, Zhang L (2016) Carboxymethyl chitosan/conducting polymer as water-soluble composite binder for LiFePO4 cathode in lithium ion batteries. J Power Sources 336: 107–114. https://doi.org/10.1016/j.jpowsour.2016.10.041
35. Lee K, Lim S, Tron A, Mun J, Kim YJ, Yim T, Kim TH (2016) Polymeric binder based on PAA and conductive PANI for high performance silicon-based anodes. RSC Adv 6(103):101622–101625. https://doi.org/10.1039/C6RA23805J
36. Mittal G, Dhand V, Rhee KY, Park SJ, Lee WR (2015) A review on carbon nanotubes and graphene as fillers in reinforced polymer nanocomposites. J Ind Eng Chem 21:11–25. https://doi.org/10.1016/j.jiec.2014.03.022
37. Bauhofer W, Kovacs JZ (2009) A review and analysis of electrical percolation in carbon nanotube polymer composites. Compos Sci Technol 69(10):1486–1498. https://doi.org/10.1016/j.compscitech.2008.06.018
38. Marsden AJ, Papageorgiou DG, Vallés C et al (2018) Electrical percolation in graphene–polymer composites. 2D Mater 5: 032003. https://doi.org/10.1088/2053-1583/aac055
39. Stauffer D, Aharony A (2018) Introduction to percolation theory, 2nd edn. CRC Press
40. Han S-W, Kim S-J, Oh E-S (2014) Significant performance enhancement of Li4Ti5O12 electrodes using a graphene-polyvinylidene fluoride conductive composite binder. J Electrochem Soc 161(4):A587–A592. https://doi.org/10.1149/2.035404jes
41. Kundu D, Krumeich F, Nesper R (2013) Investigation of nanofibrous selenium and its polypyrrole and graphene composite as cathode material for rechargeable Li-batteries. J Power Sources 236:112–117. https://doi.org/10.1016/j.jpowsour.2013.02.050
42. Zhao Y, Huang Y, Wang Q (2013) Graphene supported polypyrrole(PPY)/Li2SnO3 ternary composites as anode materials for lithium ion batteries. Ceram Int 39(6):6861–6866. https://doi.org/10.1016/j.ceramint.2013.02.020
43. Jurewicz K, Delpeux S, Bertagna V, Béguin F, Frackowiak E (2001) Supercapacitors from nanotubes/polypyrrole composites. Chem Phys Lett 347(1-3):36–40. https://doi.org/10.1016/S0009-2614(01)01037-5
44. An H, Wang Y, Wang X, Zheng L, Wang X, Yi L, Bai L, Zhang X (2010) Polypyrrole/carbon aerogel composite materials for supercapacitor. J Power Sources 195(19):6964–6969. https://doi.org/10.1016/j.jpowsour.2010.04.074
45. Nguyen MHT, Oh E-S (2015) Improvement of the characteristics of poly(acrylonitrile–butylacrylate) water-dispersed binder for lithium-ion batteries by the addition of acrylic acid and polystyrene seed. J Electroanal Chem 739:111–114. https://doi.org/10.1016/j.jelechem.2014.12.026
46. Qi Y, Nguyen MHT, Oh E-S (2020) Enhancement of the lithium titanium oxide anode performance by the copolymerization of conductive polypyrrole with poly(acrylonitrile/butyl acrylate) binder. J Appl Electrochem 50(4):431–438. https://doi.org/10.1007/s10800-020-01401-8
47. Arora K, Chaubey A, Singhal R, Singh RP, Pandey MK, Samanta SB, Malhotra BD, Chand S (2006) Application of electrochemically prepared polypyrrole–polyvinyl sulphonate films to DNA biosensor. Biosens Bioelectron 21(9):1777–1783. https://doi.org/10.1016/j.bios.2005.09.002
48. Chougule MA, Pawar SG, Godse PR, Mulik RN, Sen S, Patil VB (2011) Synthesis and characterization of polypyrrole (PPy) thin films. Soft Nanosci Lett 01(01):6–10. https://doi.org/10.4236/snl.2011.11002
49. Chen L, Bromberg L, Schreuder-Gibson H, Walker J, Alan Hatton T, Rutledge GC (2009) Chemical protection fabrics via surface oximation of electrospun polyacrylonitrile fiber mats. J Mater Chem 19(16):2432. https://doi.org/10.1039/b818639a
50. Ding A, Lu G, Guo H, Huang X (2017) Double-bond-containing polyallene-based triblock copolymers via phenoxyallene and (meth)acrylate. Sci Rep 7(1):43706. https://doi.org/10.1038/srep43706
51. Ennis BC, Truong V-T (1993) Thermal and electrical stability of polypyrrole at elevated temperatures. Synth Met 59(3):387–399. https://doi.org/10.1016/0379-6779(93)91170-7
52. Taberna PL, Simon P, Fauvarque JF (2003) Electrochemical characteristics and impedance spectroscopy studies of carbon-carbon supercapacitors. J Electrochem Soc 150(3):A292. https://doi.org/10.1149/1.1543948
53. Hu Y, Liu H, Ke Q, Wang J (2014) Effects of nitrogen doping on supercapacitor performance of a mesoporous carbon electrode produced by a hydrothermal soft-templating process. J Mater Chem A 2(30):11753. https://doi.org/10.1039/C4TA01269K
54. Aslan M, Weingarth D, Jäckel N, Atchison JS, Grobelsek I, Presser V (2014) Polyvinylpyrrolidone as binder for castable supercapacitor electrodes with high electrochemical performance in organic electrolytes. J Power Sources 266:374–383. https://doi.org/10.1016/j.jpowsour.2014.05.031
55. Moon H, Lee H, Kwon J, Suh YD, Kim DK, Ha I, Yeo J, Hong S, Ko SH (2017) Ag/Au/polypyrrole core-shell nanowire network for transparent, stretchable and flexible supercapacitor in wearable energy devices. Sci Rep 7(1):41981. https://doi.org/10.1038/srep41981
56. Eguchi T, Tashima D, Fukuma M, Kumagai S (2020) Activated carbon derived from Japanese distilled liquor waste: application as the electrode active material of electric double-layer capacitors. J

Clean Prod 259:120822. https://doi.org/10.1016/j.jclepro.2020.120822
57. Bai Y, Yin Y, Xuan Y, Han X (2020) Scalable and fast fabrication of holey multilayer graphene by microwave and its application in supercapacitors. Nanotechnology. 32(4):045602. https://doi.org/10.1088/1361-6528/abbfd4
58. Zou Z, Zhao J, Xue J, Huang R, Jiang C (2017) Highly porous carbon spheres prepared by boron-templating and reactive H 3 PO 4 activation as electrode of supercapacitors. J Electroanal Chem 799:187–193. https://doi.org/10.1016/j.jelechem.2017.06.005
59. Yang D, Jing H, Wang Z, Li J, Hu M, Lv R, Zhang R, Chen D (2018) Coupled ultrasonication-milling synthesis of hierarchically porous carbon for high-performance supercapacitor. J Colloid Interface Sci 528:208–224. https://doi.org/10.1016/j.jcis.2018.05.050
60. Mei B-A, Munteshari O, Lau J, Dunn B, Pilon L (2018) Physical interpretations of Nyquist plots for EDLC electrodes and devices. J Phys Chem C 122(1):194–206. https://doi.org/10.1021/acs.jpcc.7b10582